Title	Infrared space observatory spectroscopy of extreme carbon stars
Author(s)	Volk, K; Xiong, GZ; Kwok, S
Citation	The Astrophysical Journal, 2000, v. 530 n. 1 pt. 1, p. 408-417
Issued Date	2000
URL	http://hdl.handle.net/10722/179655
Rights	Creative Commons: Attribution 3.0 Hong Kong License

THE ASTROPHYSICAL JOURNAL, 530:408–417, 2000 February 10

INFRARED SPACE OBSERVATORY SPECTROSCOPY OF EXTREME CARBON STARS[1]

KEVIN VOLK, GUAN-ZHU XIONG, AND SUN KWOK
Department of Physics and Astronomy, University of Calgary, Calgary, Alberta, Canada T2N 1N4;
volk@iras.calgary.ca, gzxiong@iras.ucalgary.ca, kwok@iras.ucalgary.ca
Received 1999 June 18; accepted 1999 September 28

ABSTRACT

We present *Infrared Space Observatory* (*ISO*) SWS01 (2–43 μm) and LWS01 (43–195 μm) observations of five highly evolved carbon stars with extremely thick circumstellar envelopes. The unidentified 30 μm emission feature is detected in the SWS01 spectra of all five sources. This feature seems to be resolved into two subfeatures at 25.5 and 28.3 μm in two sources. These same two sources show a weak emission feature near 20 μm which may be the same as the 21 μm feature seen in carbon-rich proto–planetary nebulae. Absorption features at 13.7 μm attributed to C_2H_2 are also detected in four sources. No dust feature is detected in the LWS spectra. The only line present is the 157.74 μm line of C^+, which could be interstellar in origin.

We present radiative transfer models for the spectra of these five stars assuming that the dust is amorphous carbon. The derived optical depths at 11.2 μm range from 1.4 to 4.5, corresponding to optical depths at $V = 190$–600, making these stars among the asymptotic giant branch (AGB) stars with the most optically thick dust envelopes. From the model fittings, we found the 30 μm features to be optically thick with 5%–8% of the total stellar luminosities being emitted in the feature. For four of the five stars, the models also suggest that their mass-loss rates have been increasing rapidly over the last few 10^4 yr periods, with current mass-loss rates as high as 4×10^{-4} (D/kpc) $M_\odot$ yr^{-1}. Such high mass-loss rates imply that these stars are in the final stages of AGB evolution. The observations of these extreme carbon stars therefore represent the best cases to study the transition from AGB to proto–planetary nebulae.

Subject headings: infrared: stars — radiative transfer — stars: carbon — stars: evolution — stars: late-type — stars: mass loss

1. INTRODUCTION

Stars begin their asymptotic giant branch (AGB) evolution as oxygen-rich stars and become carbon stars as the photospheric composition of carbon exceeds that of oxgyen as the result of the dredge-up of freshly synthesized carbon from the core. Carbon stars are traditionally identified by their photospheric spectra (for a review see Wallerstein & Knapp 1998), and over 6000 carbon stars have been identified in the Galaxy (Stephenson 1989). As carbon stars ascend the AGB, they undergo increasing rates of mass loss from the surface, building up extensive circumstellar dust and gas envelopes. Although the precise mass-loss formula is not known, it is believed that the rates of mass loss increase with luminosity and can reach 10^{-5} to 10^{-4} $M_\odot$ yr^{-1} at the tip of the AGB. Such high rates of mass loss can completely deplete the hydrogen envelope before the ignition of carbon, and are responsible for the termination of the AGB. The mass-loss process also allows elements synthesized on the AGB (e.g., helium and carbon) to be ejected, therefore enriching the interstellar medium.

Recent infrared spectroscopic observations have allowed the detection of carbon stars even when their photospheres are too obscured by circumstellar extinction for optical classification (Little-Marenin et al. 1987). It has been shown that the 11.3 μm SiC circumstellar emission feature strongly correlates with the photospheric classification of carbon stars, and over 700 carbon stars have been classified by infrared spectroscopy (Kwok, Volk, & Bidelman 1997). As circumstellar extinction increases with increasing mass loss, the infrared technique becomes the only way to detect highly evolved carbon stars. The best-studied example is the infrared object IRC +10216, which has an optical brightness of only 12th magnitude (in V) but is the brightest star in the sky at the wavelength of 5 μm. As the result of self-absorption, the SiC feature in IRC +10216 is very weak. It is possible that carbon stars even more evolved than IRC +10216 exist, and such objects can be identified by their low color temperatures. The prototype of this class of objects, which we call "extreme carbon stars," is AFGL 3068. AFGL 3068 has a very low infrared color temperature ($\approx$300 K), has no optical counterpart down to a very high magnitude limit, and has no recognizable features in the 8–23 μm wavelength range covered by the *Infrared Astronomical Satellite* Low Resolution Spectrometer (*IRAS* LRS; Atlas of Low Resolution *IRAS* Spectra 1986). A group of similar objects was identified from the LRS data by Volk, Kwok, & Langill (1992). All of these sources are too faint optically to be detected in objective-prism surveys, and their carbon-rich nature is only inferred from their lack of silicate dust features in their LRS spectra. Such identification is also supported by their circumstellar chemistry as determined from molecular-line observations; CO and HCN emissions are often strong in these objects as in other carbon stars (Volk, Kwok, & Woodsworth 1993).

The extreme nature of these objects is quantitatively demonstrated by dust radiative transfer model fits to their spectral energy distributions. For the six extreme carbon star candidates in Volk et al. (1992), the derived optical depths at 11.3 μm range from 1.5 to 8. The corresponding circumstellar A_V values range from 86 to 900, depending on

[1] Based on observations made with *ISO*, an ESA project with instruments funded by the ESA member states (especially the PI countries: France, Germany, the Netherlands, and the United Kingdom) with the participation of ISAS and NASA.

the assumed dust opacity function. Such high dust optical depths imply very large mass-loss rates, which cannot be sustained for a period of more than a few times 10^4 yr before the hydrogen envelope will be completely depleted. These extreme carbon stars therefore represent objects in the last phase of AGB evolution, and are expected to evolve shortly into proto–planetary nebulae (PPNs).

The *Infrared Space Observatory* (*ISO*), with spectroscopic capabilities covering the wavelength range where most of the energy of extreme carbon stars are emitted, provided a unique opportunity to study these objects. *ISO* also extends the spectral coverage beyond *IRAS* and ground-based observations, allowing for the search of emission features that may help in the identification of the dust composition. In this paper, we report *ISO* Short Wavelength Spectrometer (SWS) and Long Wavelength Spectrometer (LWS) observations of five extreme carbon stars.

2. THE OBSERVATIONS

All these observations were done in *ISO* guest observer programs "skwok.ext_cstar" and "skwok.excst2." Table 1 lists the log of the observations. In most cases we carried out only SWS observations. For two of the brighter objects we were able to also carry out LWS observations to look for dust features in the 43 to 200 μm wavelength range.

2.1. *SWS01 Observations*

The SWS observations reported here were carried out using the SWS01 mode (resolution $\lambda/\Delta\lambda \approx 400$) of the *ISO* SWS (Kessler et al. 1996; de Graauw et al. 1996). The absolute calibration of the SWS instrument is described in Schaeidt et al. (1996). The observations were done using a 1 s reset time and 32 scan steps per set interval except for the observation of IRAS 06582+1507 where a 2 second reset time was used to get a better signal-to-noise ratio.

The spectra were all reprocessed using the Interactive Analysis Software (IAS) at the Infrared Processing and Analysis Center (IPAC) in Pasadena, California. For each source, the SWS01 reduction was carried out manually using the constituent pipeline routines (within IAS version 6.11), rather than relying on automatic processing. First, the detector-by-detector raw data were examined to identify glitches and possible dark-current problems. Detectors with high dark-current values were noted. Then the various internal routines "read_ferd," "dspd," "antimem," "dark," "updowncal," "resp_inter," "fluxcon," "flat_inter," and "extract_aar" in the IAS pipeline were applied, in the order listed.

The resulting autoanalysis results (AAR) files were read into the *ISO* Spectral Analysis Package (ISAP) for further processing. After the pipeline processing there were severe problems with level mismatches between the various SWS spectral sections. This was particularly noticeable in band 3. Two steps were used to correct this. First, the ISAP "shift" routine was used to shift the values of various bands to match a good detector. Which detector was deemed good was determined by the initial examination of the raw scans. We looked for detectors which had small dark-current levels, showed good agreement between the "up" and "down" scans, and produced smooth spectra in a given band. In addition, the "shift" routine was used to add offsets to individual lines in the data, so that the subbands agreed with each other in their overlap regions. With these procedures, we were able to obtain a smooth spectrum for each source.

Since most of our sources have no optical counterparts and are faint even at 2 μm, we had no choice but to use the lower accuracy infrared positions from the *IRAS* Point Source Catalog (PSC) or AFGL catalogs for the planning of our *ISO* observations. Since the *IRAS* positions are estimated to be no better than $\sim 20''$ and the *ISO* beam is $14'' \times 20''$, pointing errors can result in errors in the absolute fluxes of the spectra. For IRAS 19594+4047, the *ISO* observation yielded no detection at all, probably due to a poor position. In the cases of IRAS 00210+6221 and IRAS 17534−3030 the SWS01 flux density level was found to be more than a factor of 2 lower than the expected value estimated from the *IRAS* data. While most evolved AGB stars are variable sources, we do not expect so large a variation at 25 μm where the bulk of the total luminosity is radiated. The flux discrepancies are most likely due to inaccurate target coordinates. For the other objects, the flux differences between *ISO* and *IRAS* are of the order of $\pm 25\%$, and in the case of IRAS 06582+1507 the *ISO* fluxes are higher than expected from the *IRAS* photometry. Such differences can be attributed to intrinsic source variability and the uncertainties in the *IRAS* and *ISO* calibrations.

The SWS01 spectra for all the sources are shown in Figure 1. The spectra of IRAS 00210+6221 and IRAS 17534−3030 were scaled upward by factors of 2.0 and 2.3, respectively, to correct for the presumed mispointing of *ISO* during the observations. In the other cases no scaling was done.

In most cases there is good agreement in shape from 12 to 23 μm between the *ISO* SWS01 and *IRAS* LRS, but at shorter wavelengths the two data sets take on quite different shapes. Among the five sources with usable data, IRAS 06582+1507 is found to have closest overall match in shape between SWS01 and LRS. The discrepancies in shape between 8 and 12 μm cannot be due to the processing of the SWS01 spectra in ISAP, since the region of disagreement is in SWS band 2 and most of the data manipulation was done on bands 3 and 4.

Systematic calibration error cannot be ruled out because the stars in our sample are very different in spectral character from the sources used for calibration of the SWS instrument. The same comment can also be applied to the *IRAS* LRS. Keeping these uncertainties in mind, we would like to propose that the changes in spectral shape are due to real variability as a result of long-period pulsation. Since these

TABLE 1

OBSERVING LOG FOR THE *ISO* GUEST OBSERVER PROGRAMS "skwok.ext_cstar" AND "skwok.excst2"

Source	Date of Observation	Duration of Observation (s)	Mode
IRAS 00210+6221.....	1996 Dec 24	1362	SWS01
IRAS 06582+1507.....	1997 Nov 3	2624	SWS01
IRAS 17534−3030.....	1996 Mar 17	1274	SWS01
IRAS 17534−3030.....	1996 Mar 17	1161	LWS01
IRAS 19594+4047.....	1996 Mar 23	1274	SWS01
IRAS 21318+5631.....	1997 Mar 7	1274	SWS01
IRAS 21318+5631.....	1997 Mar 7	727	LWS01
IRAS 21489+5301.....	1996 Apr 24	1274	SWS01

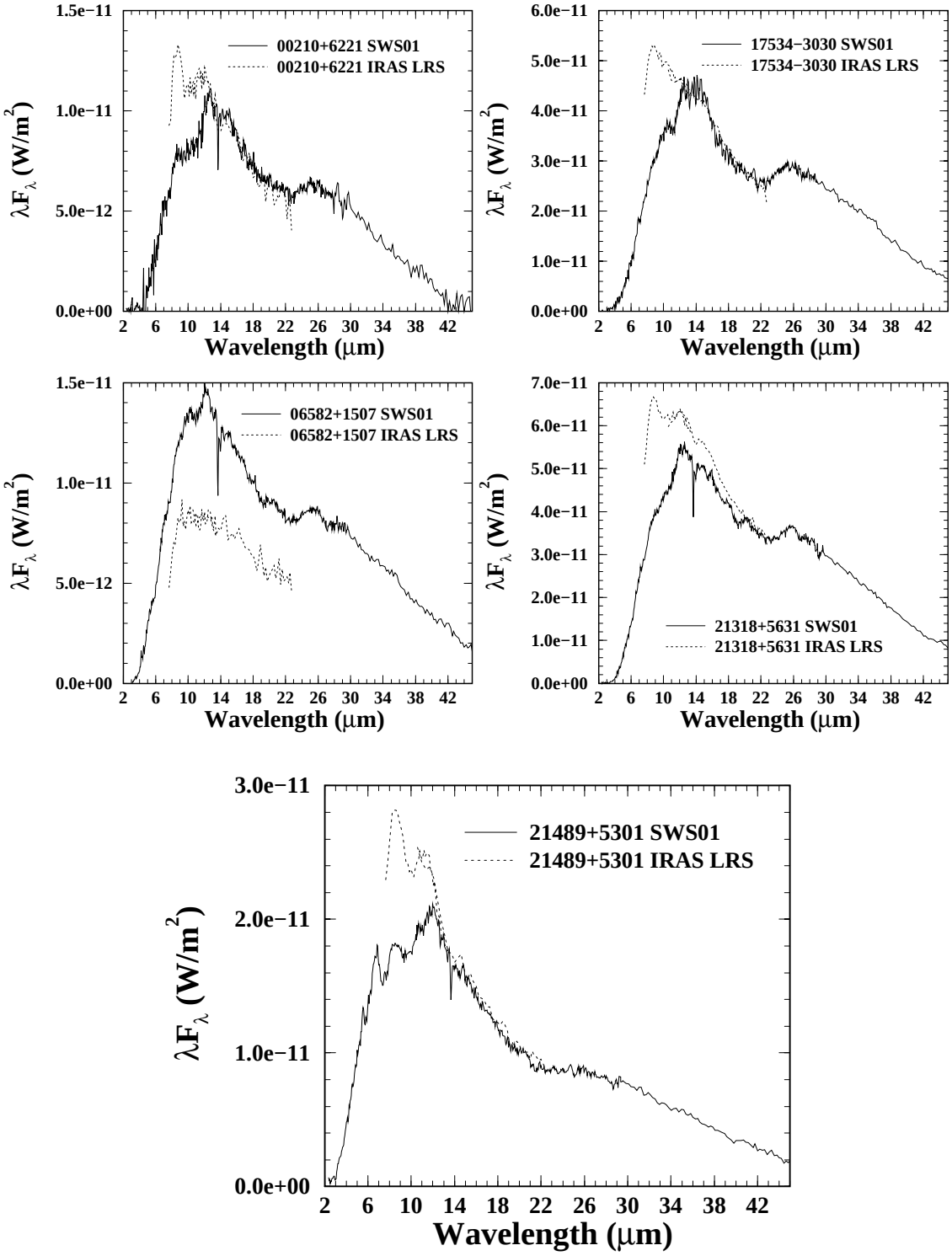

FIG. 1.—*ISO* SWS01 spectra of five extreme carbon stars. Also plotted for comparison are the *IRAS* LRS spectra.

objects are optically thick in the near- and mid-infrared, the observed difference between *IRAS* LRS and *ISO* SWS01 can be explained by a change in optical depth of the circumstellar envelope in the 13–14 years between the two observations. Alternatively, the maximum dust temperature in the circumstellar shells would have to have decreased between the time of the *IRAS* observations and the time of the *ISO* observations. Both explanations are consistent with the expected evolutionary status of these objects (see § 4).

2.2. *Features in the SWS01 Spectra*

The most dominant feature in the SWS01 spectra of these stars is the 30 μm emission feature (Forrest, Houck, & McCarthy 1981). This is a very broad feature which starts at around 22.8 μm and extends to the end of the SWS01 wavelength range. From Figure 1 we can see that the peak of the feature is at $\sim$25.3 μm. The feature is of similar shape in three sources, while IRAS 06582+1507 and

IRAS 21318+5631 show a dip at ~27 μm, splitting the feature into two separate ones.

It is possible that the local dip in the feature at 27 μm is due to an absorption feature. If so, it is centered at 27.1 μm and has a width of 2 μm. This could be absorption by another species against the background continuum of the 30 μm feature, or it could present a self-absorption of the feature itself. In the latter case, it would suggest that the optical depth of the circumstellar shell is higher in these two sources.

An alternative to the dip being an absorption feature is that there are two emission peaks, one peaking at 25.5 μm (which matches the peak for the other objects) and another peaking at 28.3 μm.

In addition to the 30 μm feature, IRAS 06582+1507 and IRAS 21318+5631 also show a weak emission feature between 19.2 and 22.7 μm. The feature has a well-defined peak at 20 μm for IRAS 21318+5631, but the peak wavelength is less certain for IRAS 06582+1507. This feature bears some resemblance to the well-known unidentified feature at 21 μm found in carbon-rich post-AGB stars (Kwok, Volk, & Hrivnak 1989; Volk, Kwok, & Hrivnak 1999), although the features in these two sources are too weak to be certain. We also note that there may be a very weak feature at 20 μm in IRAS 21489+5301.

2.3. *Molecular Absorption Lines*

In four of the five sources an absorption line at 13.68 μm is clearly seen in the SWS01 spectra. There is no trace of this line in the spectrum of IRAS 17534−3030. In IRAS 21318+5631 and IRAS 06582+1507, where the line is stronger, there is evidence for two additional lines at 13.95 and 14.44 μm. The two weaker lines are also detected at low signal-to-noise ratio in IRAS 00210+6221, while only the 13.95 μm companion line is tentatively detected for IRAS 21489+5301. A detailed analysis on these absorption lines is given in a separate paper (Xiong et al. 2000, in preparation).

2.4. *LWS01 Observations*

The LWS observations were carried out in LWS01 mode, covering the full spectral range at a resolution $\lambda/\Delta\lambda$ of $\approx$200. The instrumental characteristics are described in Clegg et al. (1996), and the calibration of the *ISO* LWS instrument is described in Swinyard et al. (1996).

The LWS01 observations of IRAS 21318+5631 and IRAS 17534−3030 were reduced using the LIA 7 package within ISAP. In this case the standard processing was carried out for each source, followed by further reduction in the ISAP package. In both cases the LWS detectors 1, 3, 4, and 9 were found to be much noisier than the others. We averaged the spectra across scans and scan direction, but not across detectors, with the default wavelength spacing of 0.135 μm, twice the actual resolution in the short-wavelength region. The averaging was done with normal clipping of outlying points. There is no significant difference whether the mean or median was used for the averaging, but the clipping reduced the resulting noise in the averaged spectrum significantly for the noisier detectors. We then carried out scaling to match the spectral sections in their overlap regions assuming that detector 0, which gave the shortest wavelength section of the LWS spectrum, was a good detector. The two LWS spectra are shown in Figure 2.

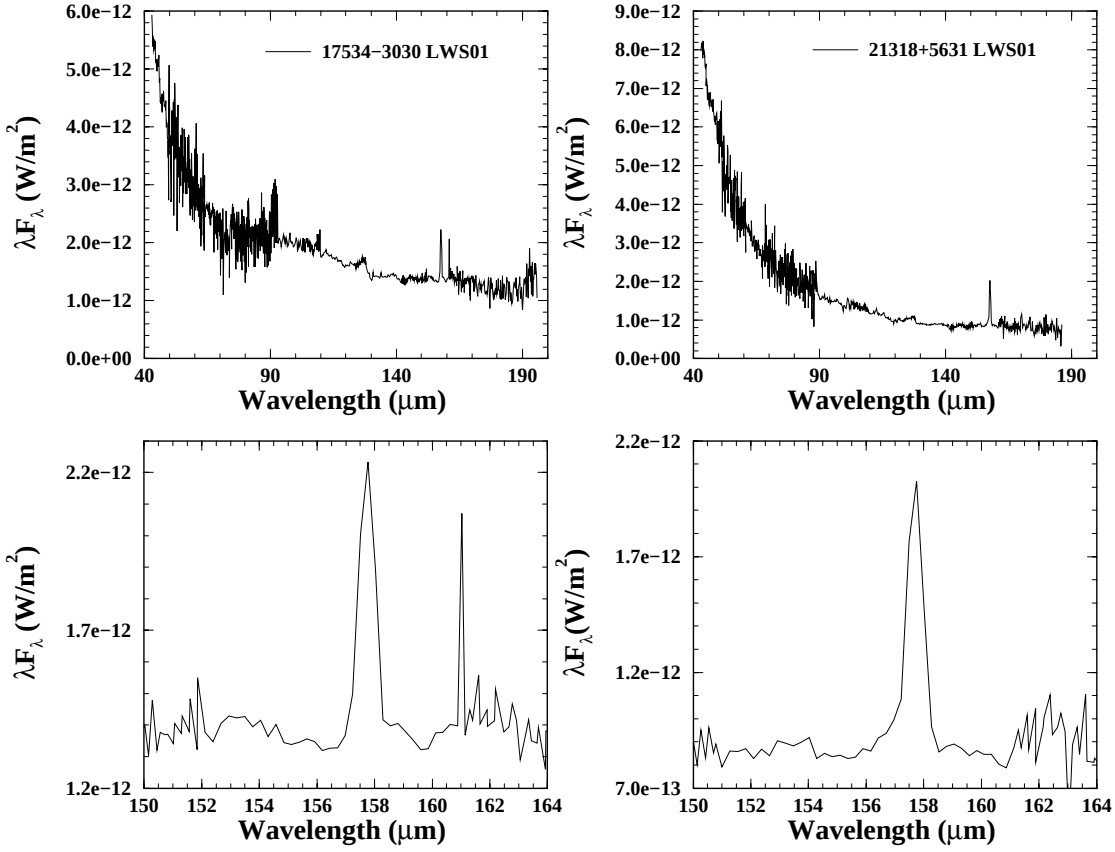

FIG. 2.—Complete LWS spectra (*top*) and expanded spectral region showing the [C II] lines (*bottom*)

Comparison of the SWS01 and LWS01 spectra in their overlap region near 43 μm showed that for IRAS 17534−3030 the LWS01 level was about a factor of 1.65 higher than that of the SWS01 spectrum. Since the *IRAS* data suggest that the SWS01 level is too low by a factor of 2.3, this suggests that the object was also not centered properly; but the off-center effect is less for the LWS than for the SWS observations. For IRAS 21318+5631 the LWS01 level is lower than the SWS01 level by 15% in the overlap region, which is reasonable given the estimated accuracy of the two calibrations ($\sim$20%).

In order to test the accuracy of the absolute flux levels of the LWS01 spectra, we convolve the observed spectra with the *IRAS* 60 and 100 μm bandpasses to produce simulated *IRAS* 60 and 100 μm photometric fluxes. In both cases the LWS01 100 μm fluxes are significantly higher than expected from the *IRAS* data. For IRAS 21318+5631 the LWS01 spectrum produced simulated *IRAS* PSC fluxes of 71.57 and 48.71 Jy at 60 and 100 μm, compared to the actual observed values of 90 ± 11 and 25.4 ± 2.5 Jy. For IRAS 17534−3030 the simulated fluxes from the LWS01 spectrum were 55.48 Jy and 65.72 Jy at 60 and 100 μm compared to observed values of 70.6 ± 7.1 and 34.5 ± 5.2 Jy. The flattening of the dust spectrum beyond 60 μm cannot be fitted by a circumstellar shell model with any reasonable dust density distribution (see § 3.3).

A careful examination of the LWS01 reduction process showed no signs of any problems, and the excess was deemed to be real. We therefore postulated that it is due to dust in the interstellar medium. This hypothesis was tested in two ways. We first estimated the excess emission by comparing the *IRAS* 60/100 μm flux density ratio and the observed LWS01 spectrum. The excess was then compared with the *COBE* FIRAS spectra[2] in the general vicinity of the stars, and the two agreed within $\sim$20%. As a second independent check, we used the ratio of the 100 μm *IRAS* point source flux density to the background as recorded in the *IRAS* PSC to get values for the total source plus background emission at 100 μm for the two objects. These values agree within the uncertainties with the simulated *IRAS* 100 μm fluxes from the LWS spectra.

On the basis of these comparisons we attribute the excess to background interstellar medium (ISM) emission. In the model fittings for these two objects in § 3.3, we used the LWS01 spectrum out to 60 μm and then used the *IRAS* PSC 60/100 μm flux density ratio to constrain the models at long wavelengths.

[2] Obtained from http://adc.gsfc.nasa.gov/ir/cobe/firas/spectr.html.

2.5. *Atomic Emission Lines*

The only strong feature in the LWS01 spectra of both sources is the fine-structure line of C^+ ($^2P_{3/2}-^2P_{1/2}$) at 157.74 μm . There is no sign of any broad dust features in the 43–195 μm wavelength range, nor do we see the crystalline silicate features that have been reported to be present in some carbon-rich stars (Waters et al. 1998). The O $^3P_1-^3P_2$ line at 63.18 μm is only marginally present.

Properties of these emission lines were derived using the line-fitting routines in ISAP, and the results are given in Table 2. These line fits were done on the original reduced data without the scaling or corrections resulting from comparison with the SWS01 data. The C^+ lines are unresolved, and the derived line widths are consistent with the spectral resolution of LWS at this wavelength. We have tried to fit the 63.18 μm line on the assumption that it is present. The line fits that resulted have only marginal significance, and required that we set the line width to 0.29 μm for the fitting. With signal-to-noise ratios of less than 3, the presence of the O I line is therefore questionable.

Since the [C II] emission line is prevalent in the Galactic plane (Wright et al. 1991), we have checked the expected background level of this line in the direction of IRAS 17534−3030 and IRAS 21318+5631 from the *COBE* FIRAS data. In neither case are the detected lines stronger than the fluxes measured by the 7° beam of *COBE*. Given the fact that interstellar dust contributes significantly to the long-wavelength fluxes of the LWS (see previous section), it is likely that the 157.7 μm emission observed in the LWS01 spectra is also primarily, or even entirely, due to the ISM.

3. MODEL FITTING TO THE DUST CONTINUUM

We have carried out dust radiative transfer models for the five sources. The initial models were carried out using a modified version of the DUSTCD code of C. M. Leung (Leung 1976). In these models we used the optical properties of amorphous carbon (AC) dust particles of radius 0.1 μm, calculated with optical constants of Rouleau & Martin (1991) for dust type 2. An empirical 30 μm feature is superimposed on the AC opacity function. The 30 μm opacity function is assumed to have a shape of an asymmetrical Gaussian with different widths (σ) for the short-wavelength and long-wavelength sides of the peak, which is assumed to be at 27.2 μm.

The stellar spectrum is assumed to be a blackbody of 2500 K. The dust is assumed to form at a condensation temperature of 1000 K. The free parameters used to fit the overall spectral shape are the total optical depth of the dust shell at 11.22 μm and the power-law index (α) of the density

TABLE 2

ATOMIC EMISSION LINES IN THE LWS01 SPECTRA

Source	λ_{peak} (μm)	Line FWHM (μm)	Line Flux (10^{-15} W m^{-2})	Peak F_λ[a] (10^{-15} W m^{-2} μm^{-1})	Continuum F_λ (10^{-15} W m^{-2} μm^{-1})	Line SNR
			[C II] 157.74 μm			
IRAS 17534−3030.....	157.74 ± 0.01	0.617 ± 0.010	3.73 ± 0.20	5.68 ± 0.20	8.71 ± 0.03	28.6
IRAS 21318+5631.....	157.70 ± 0.02	0.617 ± 0.015	4.90 ± 0.37	7.48 ± 0.37	5.65 ± 0.06	20.1
			[O I] 63.18 μm			
IRAS 17534−3030.....	63.18 ± 0.06	0.29	1.0 ± 0.4	3.3 ± 1.3	41.2 ± 0.2	2.29
IRAS 21318+5631.....	63.13 ± 0.05	0.29	1.6 ± 0.5	5.2 ± 1.6	50.0 ± 0.3	2.83

[a] Flux above the continuum.

profile

$$\rho_d(r) = \rho_d(r_0)\left(\frac{r_0}{r}\right)^{\alpha}, \quad (1)$$

where ρ_d is the dust density and r_0 is the inner radius of the dust envelope. Values of α larger than 2 imply an increase in the mass-loss rate, or a decrease in the wind speed, with time. The gas-to-dust mass ratio is assumed to be 320. The free parameters for fitting the 30 μm feature are the long-wavelength σ value and the strength of the feature in ratio to the original dust opacity function at 27.2 μm. After the shape of the SWS01 spectrum has been fitted, the model is scaled to fit the absolute flux of the spectrum and to derive the total flux ($L_*/4\pi D^2$) of the central star.

The model spectra are shown in Figure 3, and the model parameters are listed in Table 3. Two model curves are plotted: one showing the dust continuum expected from amorphous carbon grains, and the other with the 30 μm feature opacity functions added. The latter model was calculated by using the same temperature and density structures as the first model. We can see that the entire photospheric continuum of the star is absorbed by circumstellar dust and reemitted in the infrared.

From the model continuum, we have estimated the amount of energy emitted in the 30 μm feature for the

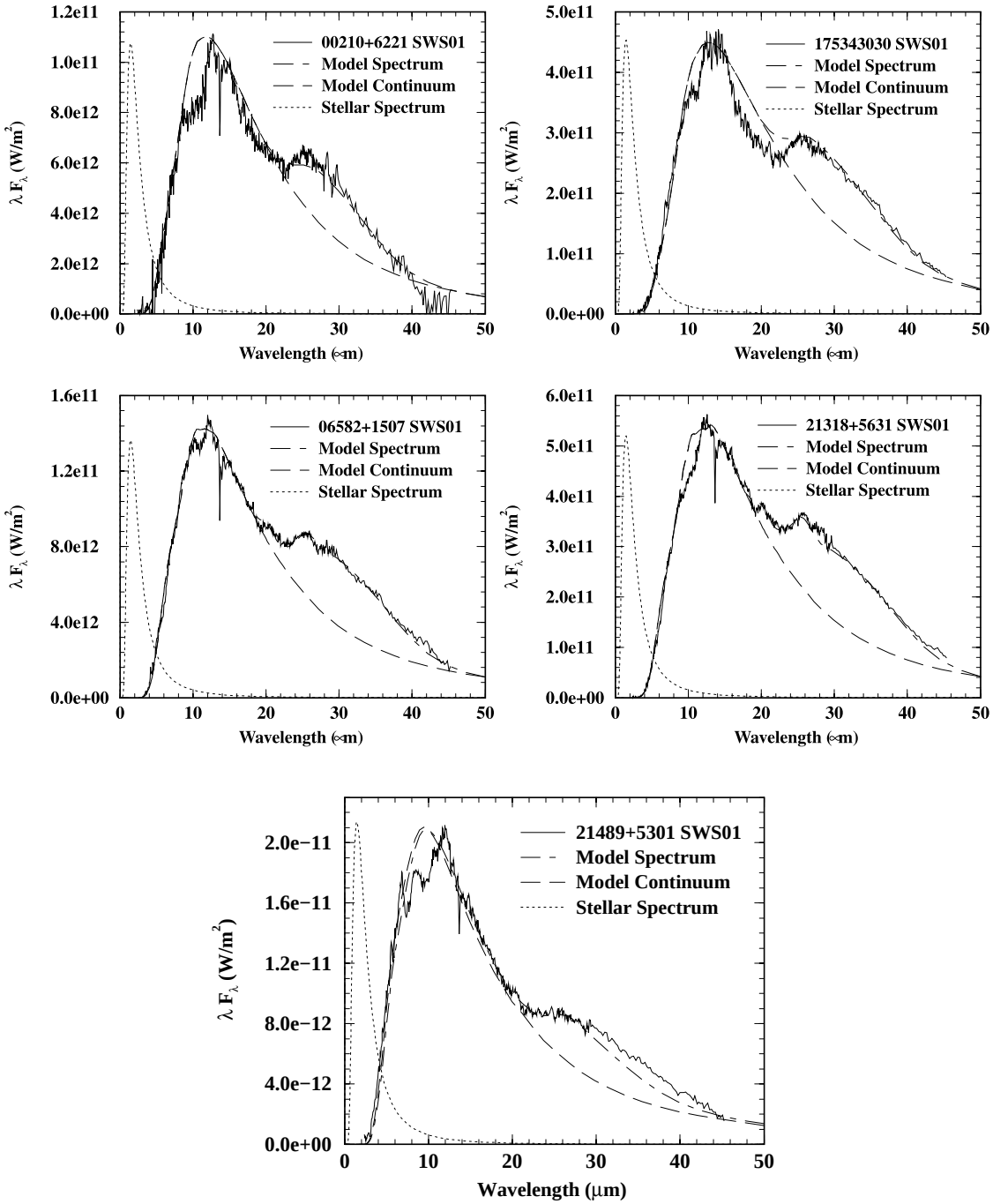

FIG. 3.—Model fits to the SWS01 spectra. The SWS01 data are shown as solid lines. Also plotted are the 2500 K blackbody stellar continua (*dotted lines*), the model AC continua (*long-dashed lines*), and the model spectra including the 30 μm feature (*dot-dashed lines*).

TABLE 3

PARAMETERS DERIVED FROM THE MODEL FITS TO THE SEDS

Parameters	00210+6221	06582+1507	17534−3030	21318+5631	21489+5301
τ (11.22 μm)	4.5	2.1	4.4	2.5	1.4
τ (0.55 μm)	596	282	583	329	189
α	3.00	2.25	2.50	2.50	2.00
r_{in}/D (10^{-5} pc kpc^{-1})	3.62	2.62	6.94	6.60	3.47
σ[a] (μm)	7.6	9.0	10.0	9.0	12.0
30 μm feature strength[b]	5.0	2.5	3.0	4.7	0.7
30 μm energy (%)	6.1	7.6	6.5	7.7%	4.9
$\dot{M}/D$ (10^{-5} $M_\odot$ yr^{-1} kpc^{-1})	12	5.5	41	22	2.8
L_*/D^2 ($L_\odot$ kpc^{-2})	450	573	1886	2143	949
V (km s^{-1})[c]	16.7	14.7 ± 2.7	31.8	16.9 ± 1.8	21.5 ± 1.2

[a] Gaussian widths of the 30 μm feature on the long-wavelength side of the peak.
[b] Feature-to-continuum ratio based on the opacity of amorphous carbon.
[c] CO expansion velocities from Loup et al. 1993, except for IRAS 00210+6221, which is from Volk et al. 1993.

sources. The derived values range from 4.9% to 7.7% of the total bolometric flux (Table 3), which are lower than the corresponding values (20%–30%) seen in PPNs (Hrivnak, Volk, & Kwok 1999). As the result of the dispersal of the circumstellar shell, dust in PPNs has lower temperatures, and the 30 μm feature is near the peak of the emission spectrum. It is likely that the 30 μm feature will strengthen when these objects evolve to the PPN phase.

3.1. *Models Taking into Account the New Dust Features*

As discussed in § 2.2, emission features in addition to the 30 μm feature can be seen in the spectra of IRAS 06582+1507 and IRAS 21318+5631. In order to take into account multiple dust features, we used a modified version of the Yorke code (Yorke 1980; see Szczerba et al. 1997) which offers certain advantages over the DUSTCD code in this respect. We used the "standard" 30 μm feature shape (with a central wavelength of 27.2 μm) and a long-wavelength σ value of 7.68 μm, and added in a new feature of Gaussian shape with a central wavelength of 25.5 μm and σ of 1.5 μm. The empirical opacity function for the 21 μm feature (derived from the feature profile of IRAS 07134+1005; Volk et al. 1999) was also included in order to fit the weak feature near 21 μm. The relative strengths of the features were then adjusted to produce the best possible fit. These models are plotted in Figure 3 for these two sources.

For IRAS 06582+1507, the feature strengths, defined as the ratio of the feature peak flux to the AC continuum, are 0.25, 0.92, and 2.5 for the 21, 25.5, and 30 μm features, respectively. In the case of IRAS 21318+5631 the corresponding values are 0.90, 4.7, and 4.7. From these models, we estimate that these features carry a total of 9.0% of the total bolometric flux of IRAS 06582+1507 and 10.2% of the total bolometric flux of IRAS 21318+5631. The models do not give a perfect fit to the feature at 20 μm, so we cannot definitely identify that as being the same as the 21 μm feature in PPNs. Because of the warmer dust continuum of these carbon stars in comparison to the PPNs, the peak of the 21 μm feature (with an opacity function peak at 20.1 μm) is shifted to $\sim$19.5 μm, whereas the observed feature peaks are at 20.0 and 20.3 μm for IRAS 21318+5631 and IRAS 06582+1507, respectively. The model fits the feature well from the peak to 23 μm in the case of IRAS 21318+5631, while in IRAS 06582+1507 the shape of the observed feature is slightly different from what the model predicts on the long-wavelength side of the peak. The feature carries 0.4% of the total emission from IRAS 06582+1507 and 0.6% of the total emission from IRAS 21318+5631 according to the models. In comparison, the 21 μm feature in the PPN IRAS 07134+1005 carries 8% of the total flux.

3.2. *Absorption Feature at 10 Microns*

All five observed sources show absorption features around 10 μm (Fig. 3). In the case of IRAS 21489+5631, two absorption features can be seen at $\approx$7.4 and $\approx$9.6 μm. It is likely that this is due to absorption by interstellar silicate dust. Due to the extreme redness of these objects, the absorption feature occurs at the peak of the spectral energy distribution rather than in the Rayleigh-Jeans side as in most other AGB stars. Consequently, the shape of the features appears to be different from the silicate profiles observed in AGB stars.

Assuming that the feature has a Gaussian profile on top of a sloped baseline, we have fitted the flux ratio of the SWS01 spectrum and the model continuum by the following formula:

$$f(\lambda) = a + b\lambda + ce^{-(\lambda-\lambda_0)^2/2\sigma^2} . \quad (2)$$

Results of the fits are given in Table 4. The fit parameters vary from object to object. The feature width is similar for IRAS 00210+6221 and IRAS 21318+5631, and 40% wider in IRAS 17534−3030. The central wavelength from the fits varies from 10.14 to 10.56 μm. There is less variation in the relative feature depth between the three sources. We were unable to obtain a satisfactory fit for IRAS 06582+1507 because the feature is weaker in this object. Assuming that the absorption feature is entirely due to absorption by cold material outside the dust shell, the optical depth (τ) of such cold dust can be derived from the depth of the feature, and the derived τ values are listed in Table 4. The assumed Gaussian absorption profile may not give a good fit if the actual feature shape is asymmetric as is the case for circumstellar silicates (Volk & Kwok 1987). We also found that the Gaussian shape did not fit the wings of the feature too well, and the widths of the features are slightly overestimated by the σ listed in Table 4.

Assuming that this feature is due to the 10 μm silicate feature in the ISM, the depths of the feature imply A_V values of 2–3 mag. Given that these objects are at relatively low Galactic latitudes and are probably at distances of 2–3 kpc, this amount of interstellar extinction is not unreasonable.

TABLE 4

FITTING PARAMETERS TO THE ABSORPTION FEATURE AROUND 10 MICRONS

Object	a	b	c	λ_0 (μm)	σ (μm)	$\tau(\lambda_0)$
00210+6221.....	0.9214	+0.0032	−0.217	10.43	0.96	0.24
17534−3030.....	1.2402	−0.0167	−0.192	10.56	1.37	0.21
21318+5631.....	0.9214	−0.0024	−0.149	10.14	0.93	0.16

3.3. *Comments on Individual Models*

We now discuss the results of the model fittings in detail for each object.

IRAS 00210+6221 ($l = 119\overset{\circ}{.}8$, $b = -0\overset{\circ}{.}1$).—The model fits the SWS01 spectrum well over most of the range from 40 μm to shorter wavelengths, but fails just at the long-wavelength end of the SWS01 range. The data values there are noisy and may not be trustworthy. There is some difference between the model and the SWS01 spectrum around the peak of the 30 μm feature. We have not been able to produce a stronger 30 μm feature in our models. If the feature opacity is made larger, it weakens the feature due to self-absorption. From 15 to 20 μm the observed continuum falls below the best-fit model continuum. This discrepancy is not as large as for IRAS 17534−3030 but is still a problem. While we could attempt to change the base amorphous carbon opacity function to match this behavior, it is not clear whether this would be physically significant given the uncertainties in the absolute calibration of the SWS01 spectra.

This object has a bright ($V = 16.51$) optical counterpart (Hrivnak, Kwok, & Boreiko 1985) and therefore may be a PPN rather than an extreme carbon star. In order to take into account this possibility, we also ran models with a detached shell with a central star temperature (5000 K) appropriate for a PPN. The results of the fit are given in Figure 4. In order to fit the optical photometry points, the total optical depth of the dust envelope must be smaller, requiring an inner radius which is ~17 times larger. At this radius, the dust temperature is 313 K. The derived mass-loss rate at the inner radius is 5.8×10^{-4} (D/kpc) $M_\odot$ yr^{-1}. The strength of the 30 μm feature is ~0.5, or 10 times smaller than in the first (nondetached-shell) model, but the fraction of energy emitted in the 30 μm feature is the same (6%). This is because in the detached-shell model, there is no warm dust in the envelope and most of the energy is radiated in the far infrared.

CO observations give an expansion velocity of 16.7 km s^{-1} and a mass-loss rate of 2.6×10^{-6} (D/kpc)^2 $M_\odot$ yr^{-1} using the standard formula from Knapp & Morris (1985) (Volk et al. 1993). Assuming that the dust is also expanding at the same velocity, the current inner radius implies that the shell was detached 36 (D/kpc) yr ago. The steep spectral shape requires a large density profile power-law index ($\alpha = 3$), which corresponds to a rapid increase of mass-loss rate with time. The CO line, being optically thick, primarily

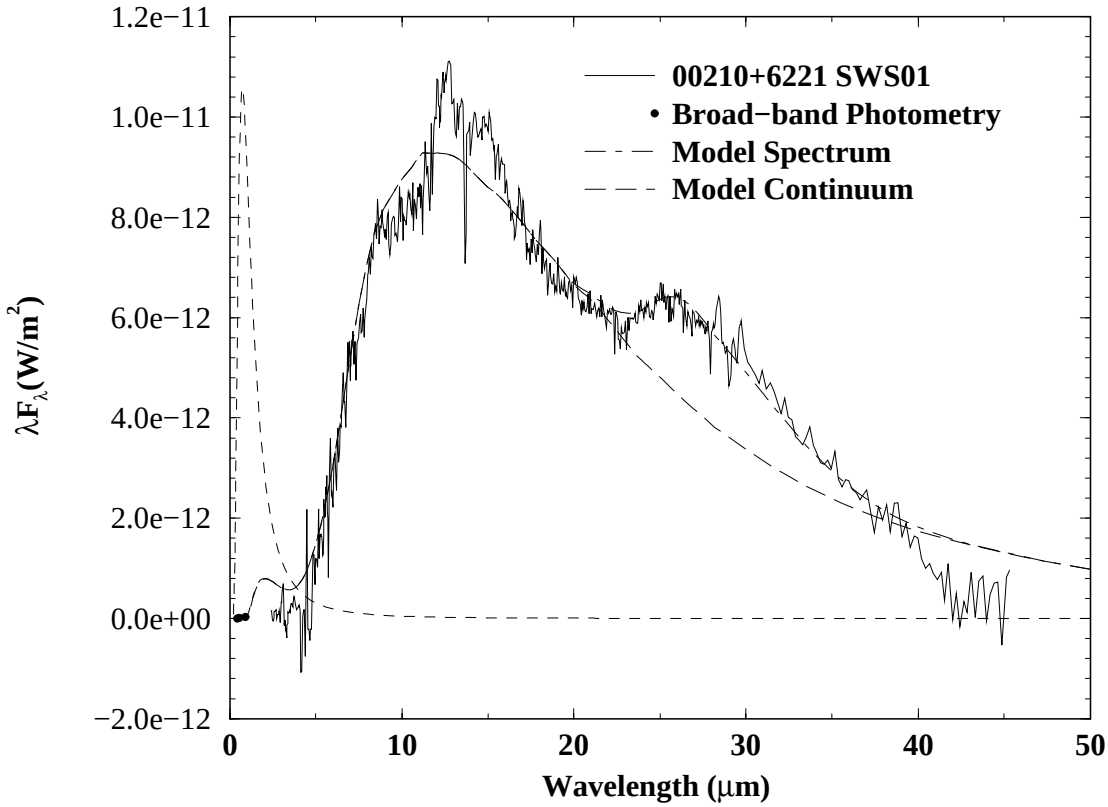

FIG. 4.—Model fit to the SED of IRAS 00210+6221 assuming a detached shell. The three filled circles on the lower left are optical (B, V, I) photometry measurements. Other symbols are as in Fig. 3. The model parameters are as follows: $T_* = 5000$ K, $\tau_{11.22\,\mu m} = 0.13$, $\alpha = 3$, $r_{in}/D = 6.2 \times 10^{-4}$ pc kpc^{-1}.

originates from the outer parts of the circumstellar envelope where the mass-loss rates are lower. This could explain the discrepancy between the mass-loss rates determined from the two different methods.

IRAS 06582+1507 ($l = 200.^\circ5$, $b = 8.^\circ9$).—In Volk et al. (1992) this source was modeled using graphite dust, and a very high optical depth was deduced. In this paper we derive much less extreme parameters and obtain a better overall fit using the amorphous carbon grains. The model predicts a change of $\dot{M}$ from 5.9×10^{-6} to 5.5×10^{-5} $(D/\mathrm{kpc})\ M_\odot\ \mathrm{yr}^{-1}$ over the past 13,000 (D kpc^{-1}) yr. The $\dot{M}$ value derived from CO observations from Loup et al. (1993) is approximately the same as the value for the outer regions.

The model produces a good fit to the whole SWS01 spectrum, with only minor discrepancies in the 10–12 μm range, around 20 μm, and around 30 μm. The general shape of the 30 μm feature matches that of the PPN IRAS 22272+5435 quite well (Szczerba et al. 1997).

IRAS 17534−3030 ($l = 359.^\circ9$, $b = -2.^\circ9$).—The model for this source does not fit the SWS01 spectrum well in the 15–20 μm region. Although not shown in Figure 3, the model fits the corrected LWS (see § 2.4) and the *IRAS* 60 and 100 μm points well. We were unable to reproduce the narrowness of the peak of the SWS01 spectrum with the standard AC opacity function. The good agreement between the *IRAS* LRS data and the SWS01 data over this region of the spectrum argues against this being due to a calibration problem. The long-wavelength width of the 30 μm feature is slightly larger than in the "standard" profile, and the strength of the feature is the largest of our five sources.

The model predicts a variation of $\dot{M}$ from 5.7×10^{-6} to 4.4×10^{-4} $(D/\mathrm{kpc})\ M_\odot\ \mathrm{yr}^{-1}$ over the past 11,000 (D/kpc) yr. Again the values from the outer part of the circumstellar shell agree with the mass-loss rate from CO by Loup et al. (1993).

IRAS 21318+5631 ($l = 98.^\circ2$, $b = 3.^\circ7$).—Here the model fits the SWS01 spectrum well except around 10 μm. Although not shown in Figure 3, the model fits the corrected LWS (see § 2) and the *IRAS* 60 and 100 μm points well. The 30 μm feature is almost as strong as in IRAS 17534−3030 and has the "standard" shape. The model suggests that $\dot{M}$ has increased from 2.8×10^{-6} to 2.1×10^{-4} $(D/\mathrm{kpc})\ M_\odot\ \mathrm{yr}^{-1}$ during the past 22,000 (D/kpc) yr. For comparison, the CO-derived $\dot{M}$ value of Volk et al. (1993) was $1.6 \times 10^{-5}\ (D/\mathrm{kpc})^2\ M_\odot\ \mathrm{yr}^{-1}$.

IRAS 21489+5301 ($l = 97.^\circ8$, $b = -0.^\circ6$).— This is the only one of our sources for which a constant $\dot{M}$ model gave a good fit to the observations. This source is also unusual in that its CO line emission is stronger than expected for the 60 μm flux density, as pointed out by Volk et al. (1993). The model spectrum fails to match the SWS01 data from 8 to 12 μm. We were also unable to match the long-wavelength part of the 30 μm feature properly even with a fairly wide Gaussian. The SWS01 spectrum has an excess compared to the model spectrum from 29 to 44 μm.

4. DISCUSSION

4.1. *Evolutionary Status*

The observations reported here leave no doubt that these cool *IRAS* sources are evolved objects with thick circumstellar envelopes. The detection of the 30 μm feature, together with the molecular absorption line of C_2H_2, strongly suggest that these stars are carbon-rich. The 21 and 30 μm feature detections also support a direct evolutionary link from these sources to PPNs and PNs. The only uncertainty is: Are these very evolved AGB stars or very young PPNs? Kwok (1993) defines PPNs as objects that are no longer undergoing large-scale mass loss but whose central stars are not yet hot enough to photoionize the circumstellar nebula. Evidence for the cessation of mass loss can be found in detached dust shells, which manifest themselves in the form of double-peaked spectral energy distributions (SEDs). As the detached shells expand, the dust temperature at the inner radius decreases and the color temperature of the object will also decrease with time. In order to give a definitive ruling on whether these objects are PPNs, we have to look at the maximum dust temperature in the circumstellar envelope of these objects. If the maximum dust temperature is much less than the expected condensation temperature of grains, we can conclude that the dust shell has been detached.

Our models have shown that the dust shells of these objects are optically thick over most of the SWS01 wavelength range. This implies that we cannot directly observe the inner regions of the dust shell, as photons emitted there are absorbed before they can escape. Consequently, the model fits are not too sensitive to the assumed dust condensation temperature of 1000 K. This is clearly illustrated in the two model fits to IRAS 00210+6221, where the inner radius in the detached-shell model (Fig. 4) is 17 times larger than the nondetached-shell model (Fig. 3). Based on the infrared spectra alone, it is very difficult to decide between these two cases. It is possible to set the maximum dust temperature at a value below 1000 K without much observational consequence except at very long wavelengths ($\lambda > 100$ μm) where the dust shells become optically thin. The only constraint on the inner radius dust temperature is the overall color temperatures of the sources, which are between 200 and 300 K. The color temperature represents the dust temperature at the radius where the 10–15 μm optical depth is unity, and it sets the lower limit to the dust temperature at the inner radius. Another constraint is set by the V extinction. If the inner radius is larger, the central star will suffer less extinction. However, in four of the five cases, the V extinction is so large that a factor of 2 or 3 decrease will have no observational consequence.

In summary, we can only say that these objects are consistent with being at the very last stage (within 10^4 yr) of the AGB, and if they have in fact evolved beyond the AGB, that must have occurred no more than one or two hundred years ago.

4.2. *Stellar Luminosities*

The SWS and LWS give excellent coverages of the spectral region where most of the fluxes are emitted by these stars, and we expect that the amount of flux missed is very small. Assuming distances of several kiloparsecs for these stars, the derived luminosities of 500–2000 $(D/\mathrm{kpc})^2\ L_\odot$ are consistent with the luminosities expected of evolved AGB stars. For example, AGB stars with core masses of 0.60 and 0.64 $M_\odot$ have luminosities of 6026 and 8318 $L_\odot$, respectively (Schönberner 1983). Given our current knowledge of the initial-final mass relationship, core masses of 0.60–0.64 $M_\odot$ correspond to main-sequence masses of 2–4 $M_\odot$. Since all five stars in our sample are located within 10° of the Galactic plane, this mass range is consistent with their loca-

tions in the Galaxy. Their thick circumstellar envelopes and carbon-rich nature resemble those of the PN NGC 7027, which could represent the evolutionary descendants of these extreme carbon stars.

4.3. *Changing Mass-Loss Rates*

One of the conclusions derived from the model fittings to the SED is the increasing rate of mass loss within the dynamical time of the observed dust envelopes. The low fluxes at long wavelengths imply that there is less mass at large distances from the star, or that less mass was ejected at earlier times. In order for the observed SEDs to be fitted by a steady stellar wind ($\alpha = 2$), one has to assume an opacity function which is much steeper than the standard AC opacity function. A counterargument to this possibility is that the model for IRAS 21489+5301 is well fitted by an inverse-square density profile. Unless we choose different grain opacity functions for each object, the conclusion of increasing mass loss is inescapable.

We should note that the fittings to the infrared spectra of these stars only derive dust mass-loss rates, and the gas mass-loss rates quoted in Table 3 are based on a gas-to-dust mass ratio of 320 and the gas velocity being equal to the dust velocity. This gas-to-dust ratio is based on a solar abundance of O, a C/O ratio of 1.4, and complete condensation into grains after the formation of CO. If the actual dust-to-gas ratio is different than assumed, then the mass-loss rates have to be adjusted accordingly.

4.4. *Geometry of the Dust Envelopes*

Most PNs have bipolar shapes, and recent observations have shown that the shaping of PNs occurs early, during the PPN phase (Kwok, Su, & Hrivnak 1998). The common belief at present is that mass loss on the AGB is largely spherically symmetric, and the shaping into bipolar shape is created by a collimated fast outflow during the PPN phase (Sahai & Trauger 1998). In this paper, a spherically symmetric dust envelope is assumed in the models. While this assumption is consistent with the above paradigm, we will nevertheless discuss the possible implications on our derived parameters if this assumption turns out to be untrue.

Since all of the five observed objects have optically thick dust envelopes, and four of the five have no visible central stars, they must be viewed edge-on if the dust envelopes are highly asymmetric. Given the relative rarity of the extreme carbon stars compared to more ordinary infrared carbon stars with the 11.3 μm SiC feature (Chan & Kwok 1990; Kwok, Volk, & Bidelman 1997), it is possible that our sample preferentially selects objects with high optical depth dust disks and nearly edge-on orientations. If this were the case, then the overall mass-loss rates averaged over all solid angles should be smaller than the values in Table 3.

5. CONCLUSIONS

The *ISO* observations reported in this paper give us a glimpse of the last moments of carbon-rich AGB stars. The SEDs of these stars are well determined by the SWS and LWS spectra, and radiation transfer model fits to the SEDs suggest that the mass-loss rates of these stars have increased rapidly in the last 10^4 yr, with current mass-loss rates exceeding $10^{-4}\ M_\odot\ \mathrm{yr}^{-1}$. Such high mass-loss rates will soon deplete the hydrogen envelope and launch the stars into the post-AGB phase of evolution. These stars are therefore likely to be the progenitors of C-rich PPNs such as AFGL 2688 (Sahai et al. 1998), and C-rich PNs such as NGC 7027. The density profiles derived here will help constrain the mass-loss formula for AGB stars as well as the dynamical models of planetary nebulae when the AGB envelopes are compressed into nebular shells under the interacting winds process.

The detection of the unidentified 30 μm feature in these extreme carbon stars shows that the material responsible for this feature is synthesized on the AGB. As the dust shell disperses during the post-AGB phase, the peak of the dust continuum spectrum will shift from $\sim$15 μm as observed in these sources to $\sim$30 μm, and the 30 μm feature will become correspondingly more prominent. Even for these extreme carbon stars, the 30 μm feature is already responsible for up to 8% of the total energy output of the stars. This puts stringent limits on what kind of material could be responsible for this feature, limiting the possibilities to compounds made up of elements of high abundance. The high spectral resolution observations presented here show that the 30 μm feature is resolved into two separate subfeatures, and these results will be important in the eventual identification of the carrier and our understanding of circumstellar chemistry.

We thank Ryszard Szczerba for helpful discussions. This work is supported by grants to S. K. and K. V. from the Natural Science and Engineering Research Council of Canada.

REFERENCES

Atlas of Low Resolution *IRAS* Spectra. 1986, IRAS Science Team, prepared by F. M. Olnon & E. Raimond (A&AS, 65, 607)
Chan, J. S., & Kwok, S. 1990, A&A, 237, 354
Clegg, P. E., et al. 1996, A&A, 315, L38
de Graauw, T., et al. 1996, A&A, 312, 511
Forrest, W. J., Houck, J. R., & McCarthy, J. F. 1981, ApJ, 248, 195
Hrivnak, B. J., Kwok, S., & Boreiko, R. T. 1985, ApJ, 294, L113
Hrivnak, B. J., Volk, K., & Kwok, S. 1999, ApJ, submitted
Kessler, M. F., et al. 1996, A&A, 315, L27
Knapp, G. R., & Morris, M., 1985, ApJ, 292, 640
Kwok, S. 1993, ARA&A, 31, 63
Kwok, S., Su, K. Y. L., & Hrivnak, B. J. 1998, ApJ, 501, L117
Kwok, S., Volk, K., & Bidelman, W. P. 1997, ApJS, 112, 557
Kwok, S., Volk, K., & Hrivnak, B. J. 1989, ApJ, 345, L51
Leung, C. M. 1976, ApJ, 209, 75
Little-Marenin, I. R., Ramsay, M. E., Stephenson, C. B., Little, S. J., & Price, S. D. 1987, AJ, 93, 663
Loup, C., Forveille, T., Omont, A., & Paul, J. F. 1993, A&AS, 99, 291
Rouleau, F., & Martin, P. G. 1991, ApJ, 377, 526
Sahai, R., & Trauger, J. T. 1998, AJ, 116, 1357
Sahai, R., et al. 1998, ApJ, 493, 301
Schaeidt, S. G., et al. 1996, A&A, 315, L55
Schönberner, D. 1983, ApJ, 272, 708
Stephenson, C. B. 1989, A General Catalog of Cool Galactic Carbon Stars (2d ed.; Publ. Warner and Swasey Observatory, Vol. 3, No. 2)
Swinyard, B. M., et al. 1996, A&A, 315, L43
Szczerba, R., Omont, A., Volk, K., Cox, P., & Kwok, S. 1997, A&A, 317, 859
Volk, K., & Kwok, S. 1987, ApJ, 315, 654
Volk, K., Kwok, S., & Hrivnak, B. J. 1999, ApJ, 516, L99
Volk, K., Kwok, S., & Langill, P. P. 1992, ApJ, 391, 285
Volk, K., Kwok, S., & Woodsworth, A. W. 1993, ApJ, 402, 292
Wallerstein, G., & Knapp, G. R. 1998, ARA&A, 36, 369
Waters, L. B. F. M., et al. 1998, A&A, 331, L61
Wright, E. L., et al. 1991, ApJ, 381, 200
Yorke, H. W. 1980, A&A, 86, 286